CrossMark

The Shannon entropy as a measure of diffusion in multidimensional dynamical systems

C. M. Giordano[1] · P. M. Cincotta[1]

Abstract In the present work, we introduce two new estimators of chaotic diffusion based on the Shannon entropy. Using theoretical, heuristic and numerical arguments, we show that the entropy, S, provides a measure of the diffusion extent of a given small initial ensemble of orbits, while an indicator related with the time derivative of the entropy, S', estimates the diffusion rate. We show that in the limiting case of near ergodicity, after an appropriate normalization, S' coincides with the standard homogeneous diffusion coefficient. The very first application of this formulation to a 4D symplectic map and to the Arnold Hamiltonian reveals very successful and encouraging results.

Keywords Chaotic diffusion · Multidimensional dynamical systems · Entropy · Rate of diffusion

1 Introduction

The characterization of chaotic diffusion in phase space of near-integrable systems is a matter of main significance in several fields, in particular, both in Celestial Mechanics and galactic astronomy. Indeed, just for the sake of illustration, we refer the reader to Maffione et al. (2015) where the relevance of chaos for halo stars in the Solar neighborhood is thoroughly discussed, and to Martí et al. (2016) which includes a careful study of diffusion in the Gliese-876 planetary system. More recently, in Cincotta et al. (2018) and references therein, a general discussion on the macroscopic diffusion is provided, as well as further applications to planetary dynamics. For instance, in Cincotta et al. (2018) the proper way to measure a

✉ P. M. Cincotta
pmc@fcaglp.unlp.edu.ar

C. M. Giordano
giordano@fcaglp.unlp.edu.ar

1 Grupo de Caos en Sistemas Hamiltonianos, Facultad de Ciencias Astonómicas y Geofísicas, Universidad Nacional de La Plata and Instituto de Astrofísica de La Plata (CONICET-UNLP), La Plata, Argentina

physical instability in a planetary system in a Laplace resonance is addressed. Meanwhile, in Martí et al. (2016) and by means of diverse chaos indicators, the motion within such a resonance was shown to be completely chaotic, though diffusion experiments revealed an almost fully stable inner part but a highly unstable outer region in the resonance.

For the sake of clarity let us state that, from now on, we will term chaotic diffusion (or just diffusion) the time variation of the prime integrals or actions of an integrable Hamiltonian due to a small non-integrable perturbation, as it is usual in dynamical astronomy.

In the above cited works, we remarked that, in the case of macroscopic diffusion, the so-called normal diffusion approximation seems not to apply in almost any near-integrable system. Such an approach assumes that a single diffusion coefficient D_w, w being any phase space coordinate, could be defined as the constant rate at which the variance of w, σ_w^2, evolves with time so that the linear trend, $\sigma_w^2 = D_w t$, is asserted. When a 2 factor is included in the definition of D, it becomes $D = \sigma^2/2t$, relationship known in physics as Fick's law, after the pioneer work of A. Fick (1855). However, when dealing with dynamical systems, the diffusion coefficient is introduced in the frame of a generalization of Brownian motion, the review by Chandrasekhar (1943) being one of the most relevant references in this field.

In fact, deviations from normal diffusion were observed in many different dynamical systems. A significant contribution to the so-called transport processes was due to Zaslavsky (see for instance Zaslavsky 1994; Zaslavsky and Abdullaev 1995; Zaslavsky et al. 1997; Zaslavsky and Niyazow 1997; Zaslavsky and Edelman 2000; Zaslavsky 2002a, b among others). Further relevant papers which pose a statistical approach are Klafter et al. (1990, 1993), Korabel and Klages (2004), Schwarzl et al. (2017), Venegeroles (2008), Miguel et al. (2014), and simple applications of such theories to planetary dynamics can be found in Zhou et al. (2002), Cordeiro and Mendes de Souza (2005) and Cordeiro (2006). Such a phenomena, called anomalous diffusion (or, more precisely, anomalous transport), affords also a characterization through the variance progression with time, which is no longer linear but of a more general form. Indeed, in the case of abnormal diffusion, the variance runs like $\sigma_w^2 = \hat{D}_w t^\beta$, where the exponent $\beta \neq 1$ strongly depends on the local dynamical structure of the deemed region of phase space. Most of the theoretical efforts concerning anomalous transport (including chaotic diffusion) considered low-dimensional systems or maps and it seems not evident how to extrapolate this statistical approach to systems of higher dimension. Indeed, the due approach to this problem is completely open to the time being.

Only in the context of normal diffusion does the derivation of a diffusion coefficient seem to be widespread in dynamical astronomy (see Cincotta et al. 2018 for more details), and the way of measuring both diffusion and its rate is far from clear in the general case. Nonetheless, suitable diffusion experiments would well serve to neatly distinguish stable and unstable regions within a chaotic domain as it was shown, for instance, in Maffione et al. (2015), Martí et al. (2016), Cincotta et al. (2018) and Maffione et al. (2018).

In the last decade, studies on diffusion in multidimensional near-integrable systems were conducted by many authors, some of them dealing with the slow diffusion regime in the limit of weak chaos (see for example Lega et al. 2003, 2008; Froeschlé et al. 2005, 2006; Efthymiopoulos and Harsoula 2013; Cincotta et al. 2014). On the other hand, diffusion studies in largely chaotic scenarios were also considered. For instance, in Tsiganis et al. (2005) and Tsiganis (2008) the diffusion theory is reviewed, including its application to the chaotic dynamics of asteroids and Jupiter's Trojans. Meanwhile, in Cachucho et al. (2010) Chirikov's formulation (Chirikov 1979; Cincotta 2002) is applied in order to derive a local diffusion coefficient within a given asteroidal three-body resonance domain, while in Batygin et al. (2015) and Martí et al. (2016) the dynamics and diffusion in the Laplace mean motion

resonance in the GJ-876 planetary system is addressed. In all cases, the normal diffusion approximation was invoked.

Herein, we recover an strategy already outlined in Cincotta and Giordano (2012), which consists on estimating the chaotic diffusion extent by recourse to the Shannon entropy. Furthermore, we provide numerical evidence that a measure of the actual mean diffusion rate could be derived from the entropy's time derivative.

In the present effort, all these issues are thoroughly discussed, first considering a well-known 4D-conservative map, where chaotic diffusion experiments are computationally much less expensive when dealing with systems of discrete time. However, we also propose the present formulation to the study of a system of continuous time, in particular, to a multidimensional near-integrable system, and present several numerical experiments regarding the $2\frac{1}{2}$ degrees of freedom Arnold Hamiltonian introduced in Arnold (1964). This system is the paradigmatic model for the so-called Arnold diffusion (actually the Arnold mechanism that leads to an instability).

2 A time discrete dynamical model

In order to show the use of the finite time entropy to quantify and measure the chaotic diffusion in a multidimensional system, we take the 4D map:

$$
\begin{aligned}
y_1' &= y_1 + \varepsilon_1 f_1(x_1) + \gamma_+ f_3(x_1 + x_2) + \gamma_- f_3(x_1 - x_2), \\
y_2' &= y_2 + \varepsilon_2 f_2(x_2) + \gamma_+ f_3(x_1 + x_2) - \gamma_- f_3(x_1 - x_2), \\
x_1' &= x_1 + \varepsilon_1 y_1', \\
x_2' &= x_2 + \varepsilon_2 y_2',
\end{aligned}
\tag{1}
$$

$x_i \in [0, 2\pi)$, $y_i \in [0, 2\pi/\varepsilon_i)$, $i = 1, 2$, where

$$
f_i(x) = \frac{\sin(x + \varphi_i)}{1 - \mu_i \cos x} - \Delta_i, \quad \Delta_i = \frac{\mu_i \sin \varphi_i}{\sqrt{1 - \mu_i^2} + 1 - \mu_i^2}, \quad \mu_i \in [0, 1), \quad i = 1, \ldots, 3,
$$

and the quantities Δ_i are fixed so that the f_i have zero average. This map has been largely discussed in Cincotta and Giordano (2016) and references therein. Rescaling the actions y_i, the map (1) becomes

$$
\begin{aligned}
y_1' &= y_1 + \varepsilon_1^2 f_1(x_1) + \varepsilon_1 \gamma_+ f_3(x_1 + x_2) + \varepsilon_1 \gamma_- f_3(x_1 - x_2), \\
y_2' &= y_2 + \varepsilon_2^2 f_2(x_2) + \varepsilon_2 \gamma_+ f_3(x_1 + x_2) - \varepsilon_2 \gamma_- f_3(x_1 - x_2), \\
x_1' &= x_1 + y_1', \\
x_2' &= x_2 + y_2',
\end{aligned}
\tag{2}
$$

where now $(x_i, y_i) \in [0, 2\pi) \times [0, 2\pi)$. In what follows, we take for simplicity $\varepsilon_1 = \varepsilon_2 = \varepsilon$, $\mu_1 = \mu_2 = \mu_3 = \mu$, $\gamma_+ = \gamma_- = \gamma$ and all the $\varphi_i = 0$, $i = 1, \ldots, 3$, so $\Delta_i = 0$.

The main difference of this 4D map from two coupled standard maps rests on the concomitant primary resonances' set. Indeed, denoting with $\hat{y}_1 = y_1/2\pi$, $\hat{y}_2 = y_2/2\pi$ and $\epsilon \equiv \varepsilon^2, \varepsilon\gamma$, up to $\mathcal{O}(\epsilon\mu^2)$, this system has the following primary resonances (see Cincotta and Giordano 2016 for details):
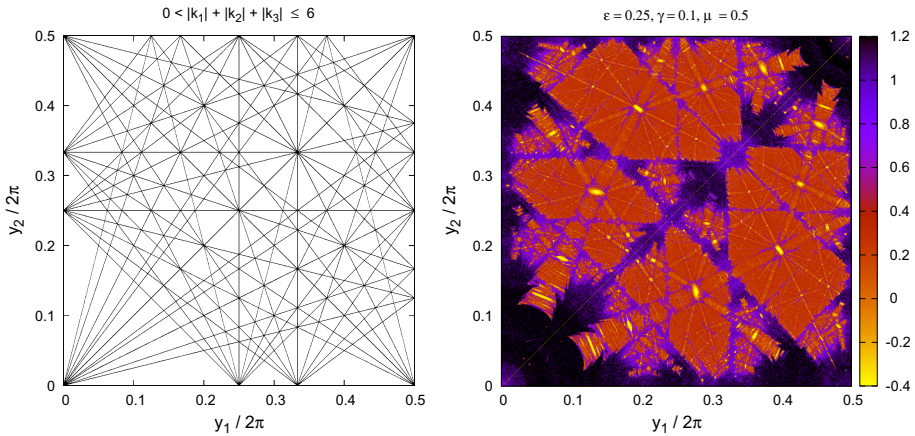
Fig. 1 On the left, the theoretical resonance web of the map (2) for $0 < |k_1| + |k_2| + |k_3| \leq 6$ and $(y_1/2\pi, y_2/2\pi) \in [0, 0.5) \times [0, 05)$. On the right, contour plot of the (logarithmic) time derivative of the conditional entropy, J, (log J values in the figure) for the map (2) with the given parameters after 400 iterates (log $2 \approx 0.3$). The initial values of the phases are fixed as $x_1 = x_2 = 0$ (see text).

$$\mathcal{O}(\epsilon): \quad \hat{y}_1, \hat{y}_2 = 0, 1;$$

$$\mathcal{O}(\epsilon\mu): \quad \hat{y}_1, \hat{y}_2 = 0, \frac{1}{2}, 1;$$

$$\mathcal{O}(\epsilon\mu^2): \quad \hat{y}_1, \hat{y}_2 = 0, \frac{1}{3}, \frac{2}{3}, 1;$$

$$\mathcal{O}(\epsilon\gamma): \quad \hat{y}_1 \pm \hat{y}_2 = 0, 1;$$

$$\mathcal{O}(\epsilon\gamma\mu): \quad \hat{y}_1 \pm \hat{y}_2 = 0, \frac{1}{2}, 1;$$

$$\mathcal{O}(\epsilon\gamma\mu^2): \quad \hat{y}_1 \pm \hat{y}_2 = 0, \frac{1}{3}, \frac{2}{3}, 1.$$

Therefore, the full set of resonances at any order in ϵ and μ is given by

$$k_1 y_1 + k_2 y_2 + 2\pi k_3 = 0, \quad k_1, k_2, k_3 \in \mathbb{Z}^+. \tag{3}$$

Thus, horizontal lines correspond to the resonances of the uncoupled (x_2, y_2) map, vertical ones to those of the uncoupled (x_1, y_1) map, while the coupling resonances are given by the lines $y_2 = -(k_1 y_1 + 2\pi k_3)/k_2$, $k_2 \neq 0$. Figure 1(left) illustrates the theoretical resonance web for $(y_1/2\pi, y_2/2\pi) \in [0, 0.5) \times [0, 05)$ for $0 < |k_1| + |k_2| + |k_3| \leq 6$.

The actual resonance web is shown in Fig. 1(right) where the final values for $t = 400$ of the (logarithmic) time derivative of the conditional entropy, J (see Cincotta and Simó 1999) have been computed for an equispaced grid of 1500×1500 pixels in the domain $(y_1/2\pi, y_2/2\pi) \in [0, 0.5) \times [0, 05)$, $(x_1(0) = x_2(0) = 0)$, since for the interval $[0.5, 1)$ it is enough to take $1 - y_i/2\pi$, with $y_i/2\pi \in [0, 0.5)$. Recall that the (symmetric) conditional entropy of nearby orbits, I, is such that $I \sim \delta_0^2 \lambda^2 t^2 \ll 1$ for stable motion, with λ the maximum linear rate of linear divergence and $\delta_0 \ll 1$ the initial value of the deviation vector; while $I \sim \delta_0^2 \exp(2\sigma t) \sim 1$ for unstable chaotic motion, where σ is the maximum Lyapunov exponent of the given trajectory. On the other hand, $J = t\dot{I}/I$ behaves like the MEGNO (Cincotta and Simó 2000; Cincotta et al. 2003; Cincotta and Giordano 2016), $J \approx 2$ for quasiperiodic motion and $J \sim \sigma t \gg 1$ for chaotic dynamics. We have chosen this

particular dynamical indicator since it provides a clear picture of the global dynamics in very short motion times due to the fact that it is of second order in the solution of the variational equations. Although I is based on a continuous entropy associated to two nearby trajectories, say γ and γ' and also to the orbit defined by $\gamma \times \gamma'$, J thus defined is quite similar to the MEGNO indicator. For further details, we refer to Cincotta and Simó (1999), while a brief discussion of both indicators is provided in Cincotta and Giordano (2016).

To clearly interpret the observed resonance structure, let us recall that the product $(x_1, y_1) \times (x_2, y_2)$ at $x_1 = x_2 = 0$ only reveals the hyperbolic 2D tori (that is, the homoclinic tangle) of the primary resonances on the (y_1, y_2) plane (as it would occur in the case of two coupled standard maps). We neatly distinguish the integer and the semi-integer resonances for the uncoupled maps as well as many coupling resonances and several high-order ones. Initial conditions that lead to strong chaotic motion take the highest values of $\log J$ while the smaller values correspond to stable quasiperiodic or periodic motion. This figure will serve later to locate the initial conditions within different chaotic domains.

In order to visualize the diffusion of any orbit onto the (y_1, y_2) plane shown in Fig. 1(right), we proceed as follows (from now on, y_i will denote $y_i/2\pi$). We take a small ensemble of n_p trajectories around some initial condition $y_1(0), y_2(0), x_1(0) = x_2(0) = 0$, iterate the ensemble during a total motion time t_f and record the intersections of the n_p orbits with the section $\mathcal{S}$ defined as $|x_1| + |x_2| < \eta \ll 1$.

Since the evolution of the variance of the ensemble is also needed, we compute the *variance over the section* (see Cincotta et al. 2018 and references therein for alternative ways of computing different variances). To this end, we take a fixed time interval $\Delta t \ll t_f$, define $t_l = l\Delta t$ and consider motion times $t_{l-1} < t \le t_l, \quad l \in \mathbb{Z}^+$. Assume that the n_p initial conditions have $n_l \gg 1$ intersections with $\mathcal{S}$ at different times $\tau_l \in (t_{l-1}, t_l]$; thus, the variance over the section is computed as

$$\Delta y_f^2(t_l) = \frac{1}{n_l} \sum_{k=1}^{n_l} \left(y_f^{(k)}(\tau_l) - y_f^{(k)}(0) \right)^2, \tag{4}$$

when the initial condition lies on a single resonance, $y_f^{(k)}$ denotes the values of the corresponding fast action (taken along the resonance line) for the ensemble. Meanwhile, for the initial conditions on multiple resonances or in a domain of resonances' overlap, we take $y_f^2 = y_1^2 + y_2^2$.

3 The Shannon entropy as a measure of chaotic diffusion

3.1 Theoretical outline and its experimental support

As we have already discussed, it is not a simple task to provide a measure of diffusion, in particular, when the latter is macroscopic. We could not invoke normal diffusion when dealing with systems of divided phase space and consequently, the derivation of a diffusion coefficient from the evolution of the variance of the unperturbed integrals is no longer valid.

Thus, in the present section we go beyond in the search of an alternative tool to this end bringing into play the finite time entropy, known as Shannon Entropy, and investigate its effectiveness for such an application. A first attempt in this direction was already given in Cincotta and Giordano (2012), while the theoretical background on the Shannon entropy can be found in Shannon and Weaver (1949); however, different approaches to the entropy in

dynamical systems are presented in for instance Katz (1967), Arnol'd and Avez (1989) and Wehrl (1978).

We will use the entropy to measure the wandering of the normalized unperturbed actions $\mathbf{y} = (y_1, y_2)$ upon a given unit square (with opposite sides identified), T, as time goes by. The adopted T corresponds to the intersections of any trajectory of the 4D map with the starting phase plane or section $|x_1| + |x_2| < \eta \ll 1$.

Following Arnol'd and Avez (1989) and Lesne (2014), consider the real-valued function Z defined in $[0, 1]$ as:

$$Z(x) = \begin{cases} -x \ln x, & x \in (0, 1] \\ 0 & x = 0. \end{cases} \tag{5}$$

Clearly, $Z(x) \geq 0$, it has a maximum at $x = \mathrm{e}^{-1}$ and $Z'' < 0$. Let

$$\alpha = \{a_i; \ i = 1, \ldots, q\} \tag{6}$$

be a partition of T, for instance, a collection of q bidimensional cells that cover the whole unit square. The elements of the partition are assumed to be both measurable and disjoint.

For any trajectory γ of the map, a probability density on T can be defined by

$$\rho(\mathbf{y}, \gamma) = \frac{1}{N} \sum_{i=1}^{N} \delta(\mathbf{y} - \mathbf{y}_i), \tag{7}$$

where $\{\mathbf{y}_i, i = 1, \ldots, N\}$ denotes the intersections of the trajectory γ with T, and δ is the delta function. It is evident that

$$\int_T \rho(\mathbf{y}) \mathrm{d}^2 y = 1, \tag{8}$$

and the measure μ of any element of the partition a_i turns out to be

$$\mu(a_i(\gamma)) = \int_{a_i} \rho(\mathbf{y}) \mathrm{d}^2 y. \tag{9}$$

Then, for the partition α the entropy of γ is defined in the fashion

$$S(\gamma, \alpha) = \sum_{i=1}^{q} Z(\mu(a_i(\gamma))) = -\sum_{i=1}^{q} \mu(a_i(\gamma)) \ln(\mu(a_i(\gamma))). \tag{10}$$

Let us notice that for a given partition and any trajectory, the entropy is bounded. Indeed, for the partition (6) it is $0 \leq S(\gamma, \alpha) \leq \ln q$. The minimum is reached when γ is restricted to a single element of α, say the k-th element, which would correspond to the case of almost full stability (for instance when all the iterates lie onto a single torus). In such a case, it is $\mu(a_k) = 1, \mu(a_i) = 0, \forall i \neq k$, yielding $S = 0$. On the other hand, the maximum value, $S = \ln q$, will be reached whenever the q elements of the partition have equal measure, $\mu(a_i) = 1/q$, that corresponds to the situation in which the unperturbed actions wander all over the unit square in a uniform fashion, i.e., in case of ergodicity. Therefore, the entropy seems to be a priori a rather natural measure of the diffusion extent.[1]

---

[1] Let us recall that Shannon entropy for a discrete-valued and discrete-time stochastic process has an analog in ergodic theory of dynamical systems; the Shannon entropy defined in (10) naturally leads to the so-called metric or Kolmogrov Sinai entropy for a given orbit of a map when considering the refinements of the partition generated by the map when $t \to \infty$, as for instance Arnol'd and Avez (1989) and Lesne (2014) show.

By means of the very same arguments given in Cincotta et al. (1999) and Cincotta (1999), if the a_i are small enough and N is large, we could assume that for any trajectory, all the non-empty elements of the partition have nearly the same measure. Thus, if q_0 denotes the number of cells visited by the orbit after a given motion time, then from (10) and the normalization condition,

$$\sum_{s=1}^{q} \mu(a_s) = \sum_{s=1}^{q_0} \mu(a_s) = 1,$$

it turns out that $\mu(a_s) \approx 1/q_0$ and

$$S \approx S_0 \equiv \ln q_0. \tag{11}$$

Therefore, under this assumption, the entropy behaves in a logarithmic way and it only depends on the fraction of the area of the unit square covered by the trajectory. Moreover, if N is large enough, q_0 would also provide an indication of the amount of instability on T. Indeed, if $q_0/q \ll 1$ we would be in presence of almost stability, while the instability would be quite large whenever $q_0/q \lesssim 1$.

The time derivative of the entropy, $\dot{S}$, can be approximated by

$$\dot{S} \approx \dot{S}_0 = \frac{1}{q_0(t)} \frac{\delta q_0}{\delta t}, \tag{12}$$

where $q_0(t)$ denotes the number of cells visited by the orbit at time t and $\delta q_0/\delta t$ the rate at which q_0 changes with time. At this point, we make the following heuristic approximation:

$$\delta q_0 \propto \langle \delta y_j^2 \rangle, \tag{13}$$

where δy_j^2 denotes either δy_1^2, δy_2^2 or $(\delta y_1^2 + \delta y_2^2)/2$ and $\langle \cdot \rangle$ is the average on T over the interval $(t, t+\delta t)$. The above estimate rests on the assumption that the variation of the occupied cells is entirely due to changes in the actions in any direction (see below).

Let us now consider two asymptotic scenarios. If γ is a stable orbit lying on a torus, then $\langle \delta y_j^2 \rangle = 0$, $\delta q_0 = 0$ and no variation of the number of cells takes place. Both the entropy and its time derivative vanish and therefore the quantity

$$S' \equiv q_0(t)\dot{S}, \tag{14}$$

also vanishes. On the other hand, in the case of a nearly ergodic system, for any trajectory it is $\delta q_0 \propto \langle \delta y_j^2 \rangle > 0$. In this particular situation, it is known that $\langle \delta y_j^2 \rangle \approx D\delta t$, where D is the homogeneous, constant diffusion coefficient of the system and thus, $S' \propto D$, so

$$S' \approx \frac{1}{k}D, \tag{15}$$

where k is a normalization constant that depends on the extreme values attained by the actions.[2] Indeed, k is chosen such that $kq_0(t)$ is the area of the action space covered by the diffusion of a given orbit.

The heuristic approximation (13) rests on the assumption that $\langle \delta y_j^2 \rangle$ is the difference in the ensemble variance on the section S at two nearby times, $\langle \delta y_j^2 \rangle = \langle \Delta y_j^2(t+\delta t) \rangle - \langle \Delta y_j^2(t) \rangle$. Then if this change in the variance satisfies $\langle \delta y_j^2 \rangle \gtrsim 1/q$, then $\langle \delta y_j^2 \rangle \sim \delta q_0$. On the other hand, if $\langle \delta y_j^2 \rangle \lesssim 1/q$, for q large enough, it is almost stability, $\langle \delta y_j^2 \rangle \ll 1$ and thus $\delta q_0 = 0$.

---

[2] Note that to compute $\langle \delta y_j^2 \rangle$ the actions are not restricted to the unit square.
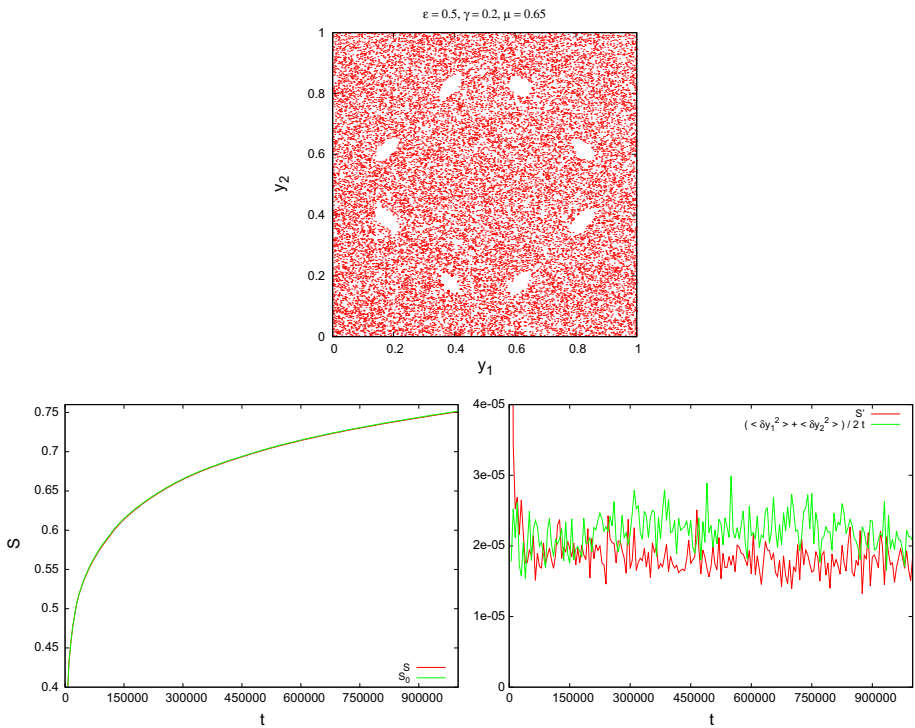
Fig. 2 Diffusion over the unit square (section $|x_1| + |x_2| \leq 0.02$) for an ensemble of size 10^{-6} of 2000 initial conditions around $(x_1, x_2, y_1, y_2) = (0, 0, 0.25, 0.25)$ for the map (2) with large values of the parameters (top panel). Entropy S and its approximation S_0 for the density distribution generated by this trajectory, both normalized by $\ln q$ (left bottom panel); S' and $(\langle \delta y_1{}^2 \rangle + \langle \delta y_2{}^2 \rangle)/2t$ (right bottom panel)

In order to test these assumptions in the case of a nearly ergodic scenario, in Fig. 2(top) we display the diffusion on the unit square, actually onto the section $\mathcal{S} : |x_1| + |x_2| \leq 0.02$, for the map (2) with values of the parameters large enough such that the system presents global and fast diffusion all over T. This plot corresponds to $t = 10^6$ iterates of the map for an ensemble of size 10^{-6} of 2000 initial conditions around $(x_1(0), x_2(0), y_1(0), y_2(0)) = (0, 0, 0.25, 0.25)$. The bottom panel (left) shows the evolution of the entropy S accordingly to (10) and its approximation S_0 given by (11), both normalized by $\ln q$, with $q = 800 \times 800$ cells of equal size. Clearly, in this particular case, both entropies completely agree. In the bottom panel at the right, we present both the temporal evolution of S' given by (15) and the time average of the variance over the section of y_1 and y_2. To compute the action variances δy, we have used (4) with $\Delta t = 5 \times 10^3$ and being $n_l \gtrsim 700$, while for S' we have taken the per step numerical change of S every Δt. To determine the constant k, we have just evaluated the maximum and minimum values attained by the actions during the iteration of the ensemble and thus

$$k = (y_{2M} - y_{2m})(y_{1M} - y_{1m}), \tag{16}$$

where y_{jM}, y_{jm} denote such maximum and minimum values, respectively. We observe that the diffusion behaves as a normal process, the rate of the variance's average approaches very quickly to a constant value leading to a diffusion coefficient, $D \approx 2 \times 10^{-5}$. This is the very same constant value of S' over the whole time interval, showing then that (15) holds.
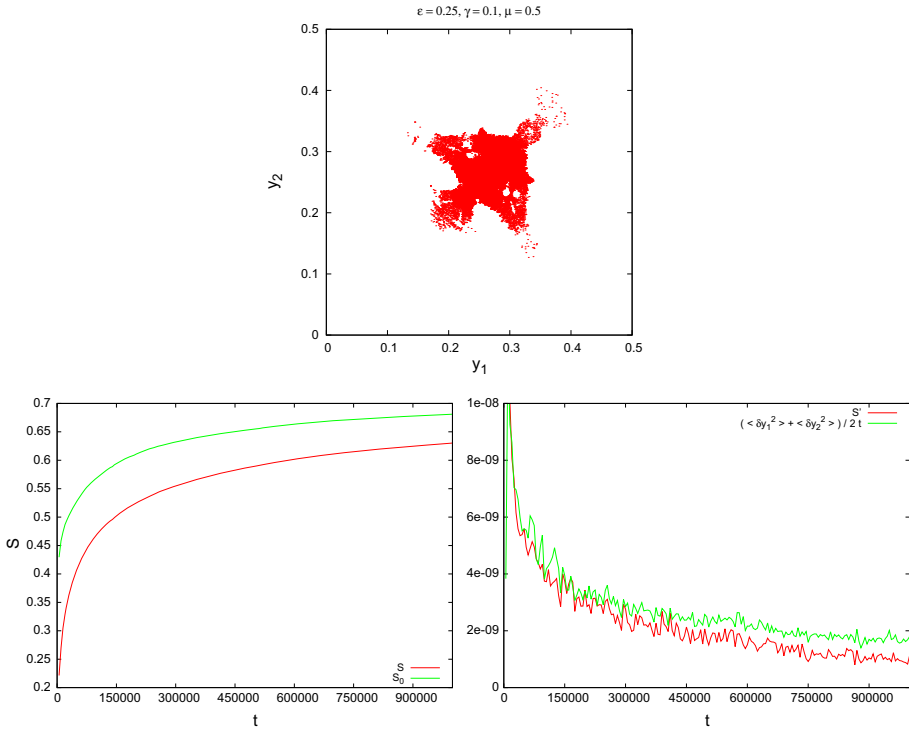
Fig. 3 Similar plot to that in Fig. 2 but for the parameters used for Fig. 1(right)

The key point of this formulation is the assumption (13), where the approximation (12) is used. It is clear that the exact form of $\dot{S}$ also involves the time derivatives of $\mu(a_i)$. Even though we have numerically computed the full derivative of S taking into account all its terms, we found that the smoothest and best approximation to $\dot{S}$ is provided by the numerical derivative of S evaluated every δt, as shown in Fig. 2. Thus, in what follows, we assume (13) to be true in any case and numerical evidence of its validity will be delivered in the next subsection.

3.2 Further Numerical experiments

In this section, we consider additional numerical experiments but involving values of the map parameters such that the resulting dynamical system presents a divided phase space, with components of comparable measure.

In Fig. 3(top), we present the results of the intersections of the same initial ensemble as in Fig. 2(top) (ensemble 1) but for the values of ε, γ and μ adopted for Fig 1(right). We have changed the partition to $q = 500 \times 500$ while the rest of the parameters (t, Δt, $\mathcal{S}$) are the same as above.

We observe that diffusion, though macroscopic, is restricted to a relatively small domain of the unit square. This is revealed by the values of the concomitant entropies that are smaller than those for the case in which the system covers almost all the unit square; however, here the size of the cells of the partition is larger. Note that though the normalized entropies, S and S_0 somewhat depart, both evolve at a similar rate. We can provide a rough estimate of
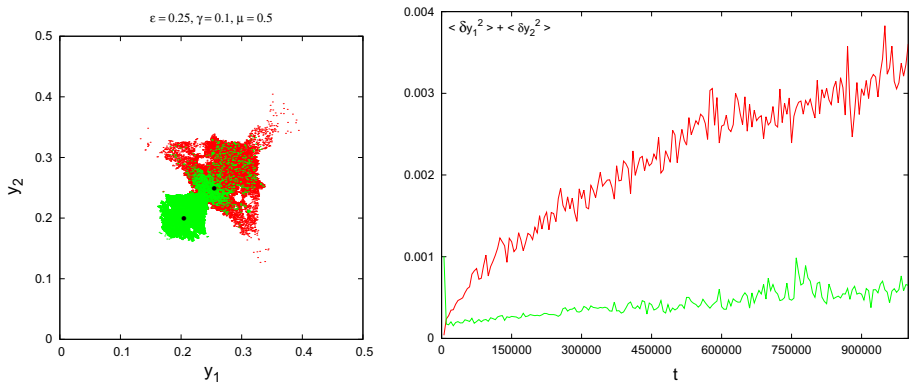
Fig. 4 (Left panel) Diffusion observed up to 10^6 for two ensembles of size 10^{-6} of 2000 initial conditions, one (in red) starting at $(y_1(0), y_2(0)) = (0.25, 0.25)$, the same as Fig. 3(left panel) but plotted with half of the crossings with $\mathcal{S}$, and a second one (in green) initially located at $(y_1(0), y_2(0)) = (0.20, 0.20)$. The black squares indicate the location of the initial ensembles. (Right panel) Variance evolution $\langle \delta y_1^2 \rangle + \langle \delta y_2^2 \rangle$ for both ensembles with the same color identification

the extent of the diffusion recalling that, for the normalized entropy it is $q_0 \approx q^S$ and being the size of the cells $1/q$, the area covered by the ensemble is $q_0/q \approx q^{S-1}$ and therefore the linear extension of the diffusion would be $\Delta y_i \sim q^{(S-1)/2}$, for $q = 500 \times 500$ and after 10^6 iterates, $S \approx 0.65$, leading to $\Delta y_i \sim 0.11$. The right panel reveals that, even in the case of a bounded diffusion, Eq. (13) holds. The constant k in (15) is obtained again by recourse to (16). We observe that the mean rate at which the variances evolve with time is still slowly decreasing at $t = 10^6$, revealing that the diffusion is not normal over this time interval.

In view of the above results and those of our vast numerical experimentation, we here propound S and S' as an indication of the extent of the diffusion and the rate at which it changes, respectively, the latter providing a measure of the macroscopic diffusion rate. In this direction, we focus on the next experiment.

Fixing again $\varepsilon = 0.25$, $\gamma = 0.1$ and $\mu = 0.5$, we take a similar ensemble as the one above, but now centered at $(x_1(0), x_2(0), y_1(0), y_2(0)) = (0, 0, 0.20, 0.20)$ (ensemble 2). A simple inspection of Fig. 3 (left panel) reveals that the ensemble 2 lies on the region covered by the diffusion starting at $y_1(0), y_2(0) = (0.25, 0.25)$ (ensemble 1) so that we should expect similar dynamical properties for both ensembles, that is comparable variance evolution and diffusion rates.

Figure 4(left) shows that the diffusion of both ensembles, though with a different surface density distribution, their corresponding areas largely overlap; however, their variances evolve in a quite different way, as Fig. 4(right) shows. Again, it is evident that the observed diffusion is not normal and thus any attempt to estimate a diffusion coefficient, for instance by a linear fit on the variance evolution, would lead to very dissimilar values for such a macroscopic instability.

Now, Fig. 5(left) shows the evolution of the normalized entropies for both ensembles. As expected, the final value of S for ensemble 1 is larger but comparable to that of ensemble 2, since the intersections of the latter with the section seem to be more confined than those of ensemble 1. Also they evolve in a different way and note that at $t \approx 1.5 \times 10^5$ both entropies take the very same value. For $t > 1.5 \times 10^5$ the entropy for ensemble 2 slightly varies, while for ensemble 1 it is still increasing, revealing that diffusion continues visiting new cells of phase space. The evolution of S' for both ensembles also reveals that the measure of the rate
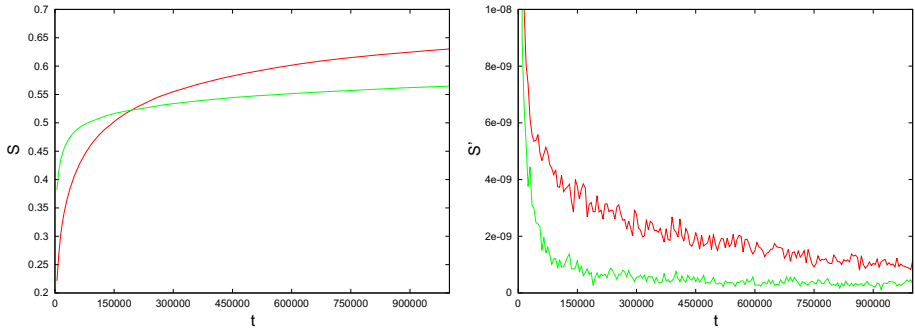
Fig. 5 Evolution of S and S' for the ensembles 1 and 2, each identified with the same color pattern as in Fig. 4

of this macroscopical diffusion should be comparable, and in fact, their final values are rather similar. In both cases, the diffusion rate would be close to 10^{-9} after $t = 10^6$.

Several numerical experiments have been carried out with different values of the map parameters, in particular for very small, moderate and large values of ε, γ and μ. Also the total motion time ranged from $t = 10^4$ to $t = 10^7$, with different selections of Δt, for ensembles located all over the unit square and considering different partition sizes. The results concerning $S(t)$, $S'(t)$, $q_0(t)/q$ and variances' evolution are quite well represented by the results shown in Figs. 4 and 5.

Finally, as a global experiment and adopting again $\varepsilon = 0.25$, $\gamma = 0.1$, $\mu = 0.5$ we take a grid of 500×500 initial values of $(y_1, y_2) \in [0, 0.5) \times [0, 0.5)$ with $x_1(0) = x_2(0) = 0$. We consider ensembles of size 10^{-7} of 10 initial conditions around each $y_1(0)$, $y_2(0)$ and compute the corresponding final values of S, S' and q_0/q on the section $\mathcal{S} : |x_1| + |x_2| \leq 0.02$, with $q = 500 \times 500$ and after a total motion time $t = 5 \times 10^5$, taking $\Delta t = 2.5 \times 10^3$. In order to reduce oscillations in the final value of S' as Fig. 5(right) shows, we average the values of S' over the interval $(5\Delta t, t)$.

Figure 6 displays the results for S and S' (in logarithmic scale). Both figures should be compared with Fig. 1(right), but keeping in mind that while the chaos dynamical indicator J has been obtained for $t = 400$, the entropy computation involves $t = 5 \times 10^5$ so that around resonances and their crossings the chaotic domains become larger, as both S and S' contour plots reveal. Recall that due to computational limitations Fig. 6 has 11% of the resolution of Fig. 1(right). Although the global picture given by the three figures is similar, note that while J measures the local exponential rate of divergence around each initial condition $y_1(0)$, $y_2(0)$, S and S' provide a measure of the extent and the rate of diffusion of a small ensemble starting at $y_1(0)$, $y_2(0)$, respectively. As we observe from these figures, for the map (2) and the given values of ε, γ and μ, the mean diffusion rate ranges from $\log S' \lesssim -13$ to $\log S' > -10$. Note that the lower values of S' correspond to stable, regular motion where the expected value is $S' \approx 0$ while the larger ones appear in chaotic domains of the phase space. The most unstable region corresponds to the intersection of the two half integer resonances $y_1 = y_2 = 0.5$, while around the integer resonances' crossing the diffusion rate is clearly smaller and certain dynamical structure is revealed by both S and S'. The lower values of the (normalized) entropy are very close to 0 as expected; on the other hand the highest values are nearly half of its maximum value, so every ensemble of orbits with $S \sim 0.5$ visits $\sim \sqrt{q} = 500$ cells of size 4×10^{-6} in 5×10^5 units of time, leading to a linear extension of the larger instability of the order of 0.05. A very similar (not included) figure is obtained for the contour plot of q_0/q, revealing that this simple ratio also provides a measure of the extent of diffusion.
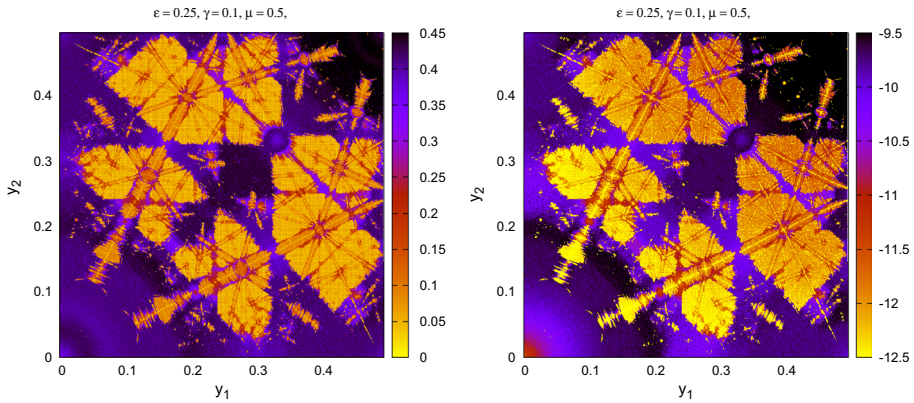
Fig. 6 Contour plot for S (left) and S' (right, in logarithmic scale) for a grid of 500×500 initial conditions and taking ensembles of 10^{-7} containing 10 values of $y_1(0)$, $y_2(0)$ around the equispaced grid values after $t = 5 \times 10^5$ (see text for more details)

The question is why S and S' yield a better estimation of the diffusion extent and its mean rate than those derived for instance from the variance (4). The answer seems to be quite simple. The variance evolution of the ensemble is highly sensitive to stickiness and this phenomena seriously affects its time rate, as for instance Fig. 4 clearly shows. As a consequence, any estimation of a diffusion coefficient computed over a finite time interval by means of a normal diffusion assumption would in general fail.[3] On the other hand, the entropy, which takes into account all the dynamical information of the ensemble trajectory, evolves in a smooth way and it is much less affected by stability domains that slow down the chaotic diffusion during some time interval. Essentially, the entropy measures the full area of the intersections of the orbits with the section $\mathcal{S}$. Of course, the intrinsic time dependence of the diffusion due to the dynamical phase space structure and its anisotropic character are also observed by means of the entropy. The same arguments apply to S' and thus we are confident of S and S' to provide a good measure of the chaotic diffusion within a given finite time interval.

4 A continuous time dynamical system: the Arnold model

The classical Arnold Hamiltonian (Arnold 1964) (also discussed in Chirikov (1979), Giorgilli (1990), Simó (2001), Lega et al. (2008), Efthymiopoulos (2012) among many others) has been recently revisited in Cincotta et al. (2018) and herein we follow its approach. The Hamiltonian has the form

$$H(I_1, I_2, \theta_1, \theta_2, t; \varepsilon, \mu) = \frac{1}{2}\big(I_1^2 + I_2^2\big) + \varepsilon(\cos\theta_1 - 1)(1 + \mu\mathcal{B}(\theta_2, t))$$
$$\mathcal{B}(\theta_2, t) = \sin\theta_2 \ + \ \cos t, \tag{17}$$

with $I_1, I_2 \in \mathbb{R}, \quad \theta_1, \theta_2, t \in \mathbb{S}^1$, where μ should be exponentially small with respect to ε, for any analytical approach.

---

[3] The estimation of the exponent β and the corresponding diffusion coefficient by a power law fit seems not to work when dealing with such finite times, the value of β being highly sensitive to both the total motion time and Δt (see however next section).

For $\varepsilon = 0$ the system has two global integrals of motion, namely I_1 and I_2, which determine the invariant tori supporting the quasiperiodic motion with frequencies $\omega_1 = I_1$, $\omega_2 = I_2$. In case $\varepsilon \neq 0$, $\mu = 0$ the system still has two integrals,

$$H_1^\varepsilon(I_1, \theta_1) = \frac{1}{2}I_1^2 + \varepsilon(\cos\theta_1 - 1), \qquad I_2, \tag{18}$$

and the unperturbed Hamiltonian takes the form

$$H_0^\varepsilon(I_1, I_2, \theta_1) = H_1^\varepsilon(I_1, \theta_1) + \frac{1}{2}I_2^2. \tag{19}$$

The Hamiltonian H_1^ε is the pendulum model for the resonance $\omega_1 = 0$; $H_1^\varepsilon \equiv h_1 = -2\varepsilon$ corresponds to the exact resonance or stable equilibrium point at $(I_1, \theta_1) = (0, \pi)$ while $h_1 = 0$ to the separatrix and thus $(I_1, \theta_1) = (0, 0)$ is the unstable point. The frequencies are then

$$\omega_1 = \omega_p(h_1, \varepsilon), \quad \omega_2 = I_2,$$

where $\omega_p(h_1, \varepsilon)$ denotes the pendulum frequency. Close to the separatrix, for both oscillations and rotations, $\omega_p(|h_1| \ll 1, \varepsilon) \equiv \omega_{sx}(h_1, \varepsilon) \to 0$ when $|h_1| \to 0$. The half-width of the resonance $\omega_1 = 0$ in action space is $(\Delta I_1)^r = 2\sqrt{\varepsilon}$, so within this resonance the variation of I_1 is bounded by $|\Delta I_1| \leq 2\sqrt{\varepsilon}$ while I_2 remains constant. Therefore in action space, $\omega_1 \to \omega_{sx}(h_1, \varepsilon) \to 0$ when $I_1 \to 2\sqrt{\varepsilon}$ ($h_1 \to 0$).

For $\varepsilon \neq 0$, $\mu \neq 0$ the full system (17) can be recast as

$$H(I_1, I_2, \theta_1, \theta_2, t; \varepsilon, \mu) = H_0^\varepsilon(I_1, I_2, \theta_1) + \mu V^\varepsilon(\theta_1, \theta_2, t),$$
$$\mu V^\varepsilon(\theta_1, \theta_2, t) = \varepsilon\mu(\sin\theta_2 + \cos t)(\cos\theta_1 - 1), \tag{20}$$

where H_0^ε is given by (19) and $\theta_2(t) = \omega_2 t + \theta_2^0$. The perturbation μV^ε, for $\varepsilon\mu \ll 1$, mainly affects the motion close to the separatrix of the resonance $\omega_1 = 0$ leading to the formation of the chaotic layer; the dynamics becomes unstable, chaotic in a small domain $|I_1 \pm 2\sqrt{\varepsilon}| \leq w_s$, where w_s denotes the width of this layer. However, due to the dependence of V^ε on θ_2, also I_2 changes, and therefore motion along the stochastic layer could proceed. Due to the chaotic character of the dynamics inside this narrow layer, the variation of I_2 should also be chaotic, giving rise to variations in I_2. Thus, as I_2 could change unboundedly, a large instability might exist. This is the way in which Arnold diffusion is discussed in Chirikov (1979).

In (20) $\omega_1 = 0$ is just one of the six first-order resonances involved. A simple trigonometric manipulation reveals that the resonances at order ε and $\varepsilon\mu$ are

$$\omega_1 = 0, \quad \omega_2 = 0, \quad \omega_1 \pm \omega_2 = 0 \quad \omega_1 \pm 1 = 0. \tag{21}$$

The resonances intersect at seven different points in frequency space, namely $(\omega_1, \omega_2) = (0, 0), (0, \pm 1), (\pm 1, \pm 1),$[4] hence the diffusion would spread over all this resonance set. However for $\varepsilon\mu \ll \varepsilon \ll 1$ the diffusion rate should be negligible along all resonances except for $\omega_1 = 0$, since the latter has the main amplitude $\sim \varepsilon$, while all the other resonances have amplitudes $\sim \varepsilon\mu \ll \varepsilon$.[5]

Considering the fully perturbed motion, besides the ones given in (21), the full set of resonances (in action-energy space) is given by a linear combination of the form

$$m_1\omega_p(h_1, \varepsilon) + m_2 I_2 + m_3 = 0, \quad m_1, m_2, m_3 \in \mathbb{Z}. \tag{22}$$

---

[4] Note that their intersections in action space is different.

[5] It is well known that the theoretical diffusion rate depends exponentially on $-1/\sqrt{V_{mn}}$ where V_{mn} stands for the amplitude of the above considered resonances.

In Cincotta et al. (2018) portraits similar to those displayed in Fig. 1 are included showing the resonance web defined by (22) and a MEGNO dynamical map for this model.

4.1 Numerical experiments

Let us investigate the diffusion in this model by fixing the value of $\varepsilon = 0.25$ and taking two different values of $\mu = 0.01, 0.025$. We will focus on chaotic diffusion along the stochastic layer of the main or guiding resonance, $\omega_1 = 0$, and for different initial values of $\omega_2 = I_2$. According to Chirikov's theoretical results Chirikov (1979) by means of the normal diffusion approximation, when $\mu\varepsilon \ll \varepsilon \ll 1$ the local diffusion rate for $|\omega_2| < 1$ should be larger than for $|\omega_2| > 1$. As pointed out in Cincotta et al. (2018), this difference in the diffusion rates rests on the assumption that for $|\omega_2| < 1$, the strongest perturbation to the motion on the separatrix of the guiding resonance is due to the closest resonance in frequency space, the layer resonances $\omega_2 = \pm\omega_1$ that give rise to the chaotic layer around the separatrix of the guiding resonance (motion across the layer), and thus the diffusion along this layer is driven by the smaller perturbing terms, the driving resonances $\omega_1 = \pm 1$. For $|\omega_2| > 1$, the layer resonances turn to $\omega_1 = \pm 1$, while the driving resonances become $\omega_2 = \pm\omega_1$. Clearly, near $|\omega_2| = 1$ all these arguments are no longer applicable as well as when $\varepsilon \lesssim 1$, so for the adopted values of ε, μ and for $|\omega_2| \approx 1$ numerical experiments are required.

For $\varepsilon = 0.25$, the unperturbed separatrix (or the center of the chaotic layer) of the guiding resonance lies at $I_1 = 1$ and typical time scales for the motion inside the chaotic layer are $T_a \lesssim 20$ (see Cincotta et al. 2018). We focus on the diffusion within a range of $|\omega_2|$ where the guiding, layer, driving and other high-order resonances exhibit crossings and overlapping as the MEGNO contour plots reveal in Figs. 7 and 8, e.g., $|\omega_2| \leq 2$.

We took action values on the chaotic layer, $(I_1, I_2) = (1, \omega_2)$, and $\theta_1 = \pi, \theta_2 = t = 0$ as the initial values for the angle variables, in coincidence with those adopted for computing the MEGNO map. We considered six ensembles of 100 initial values of the actions around $(1, \omega_2)$ of size $\sim 10^{-7}$ for each value of μ. The center of each ensemble lies at $\omega_2 = -1.69, -1.13, -0.173, 0.053, 0.55, 1.55$, respectively. The equations of motion were integrated with a time step of size 0.01 for a total motion time 4×10^6.

The results for $\mu = 0.025$ are reported in Fig. 7, where the wandering of the actions for the initial ensemble (depicted in white) is pursued and superimposed on the MEGNO contour plot (for $|I_1| \leq 1.5, |I_2| \leq 2$), each color identifying a different set of 100 trajectories. In order to observe the diffusion in the 2D plane (I_1, I_2), we considered the section defined by $|\theta_1(t) - \pi| + |\theta_2(t)| < 0.01$.

From these experiments, we observe that despite the location of the initial ensemble, the diffusion spreads over the range $|I_2| \leq 2$ almost uniformly and in all cases the same resonances are visited after the considered motion time. Then, for these values of ε and μ, the instability is large and it is expected the same mean diffusion rate all over $|I_2| \lesssim 2$.

The results for $\mu = 0.01$ are presented in Fig. 8, where we observe that the ensembles located at the lowest and highest values of ω_2 reveal a bounded diffusion over the range $0.4 \lesssim |I_2| < 2$, while for the rest of the ensembles the diffusion spreads over a barely smaller domain than that for the case of $\mu = 0.025$, $|I_2| < 2$. Therefore, for these four ensembles, we also expect a similar characterization of the diffusion, as well as for the ensembles located at $\omega_2 = -1.69, 1.55$.

Figure 9 presents the variance evolution of the ensembles over the section $|\theta_1(t) - \pi| + |\theta_2(t)| < 0.01$ computed by means of (4) for $\Delta t = 2 \times 10^4$ ($n_l \gtrsim 1000$). We observe that for $\mu = 0.025$ the diffusion does not behave in a normal fashion; moreover, fitting a power law provides quite different exponents ranging from 0.10 to 1.02 when considering the full
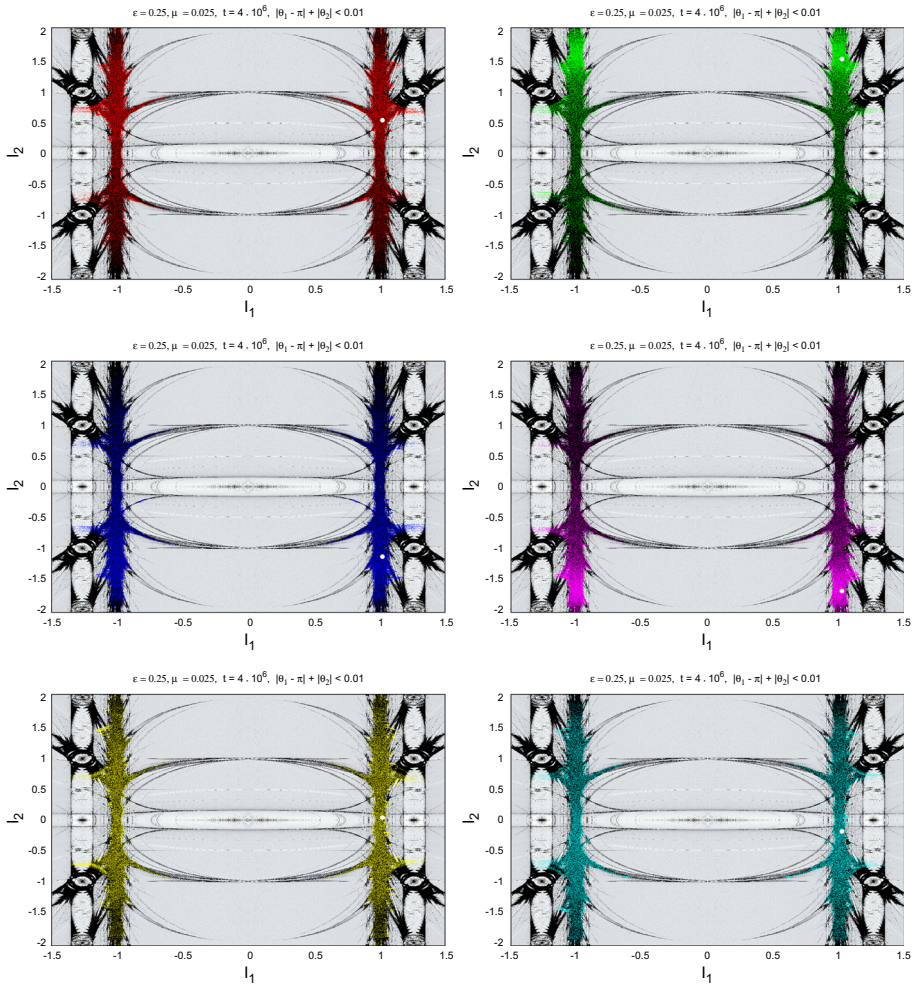
Fig. 7 Six initial ensembles (indicated as white circles) are followed onto the MEGNO contour plot for $\epsilon = 0.25$, $\mu = 0.025$, white and light gray denote stable motion while black indicates strong chaotic dynamics. The concomitant trajectories for the six ensembles that intersect the section $|\theta_1(t) - \pi| + |\theta_2(t)| < 0.01$ are depicted with different colors. Figure taken from Cincotta et al. (2018)

time span. However, when the last 80% lapse is regarded, lower exponents are obtained in some cases. Similar results arise for $\mu = 0.01$, although the variance's evolution seems to be closer to that corresponding to a normal process: a power law fit provides exponents in the range $0.63 - 0.8$ for the ensembles that present a more extended diffusion and close to 1 for the other ones. Therefore, the characterization of the diffusion by means of the variance evolution over the considered time-scale seems not to represent what it is observed in Figs. 7, 8, since in almost all cases the dynamical properties of the system for each value of μ should be very similar.

A region in action space encompassing all the crossings with the section has to be determined in order to define a partition for the computation of S and S'. Here we take $L_1 = \{I_1 : |I_1| \leq 1.4\}$, $L_2 = \{I_2 : |I_2| \leq 2.5\}$ for $\mu = 0.025$, while $L_1 = \{I_1 : |I_1| \leq$
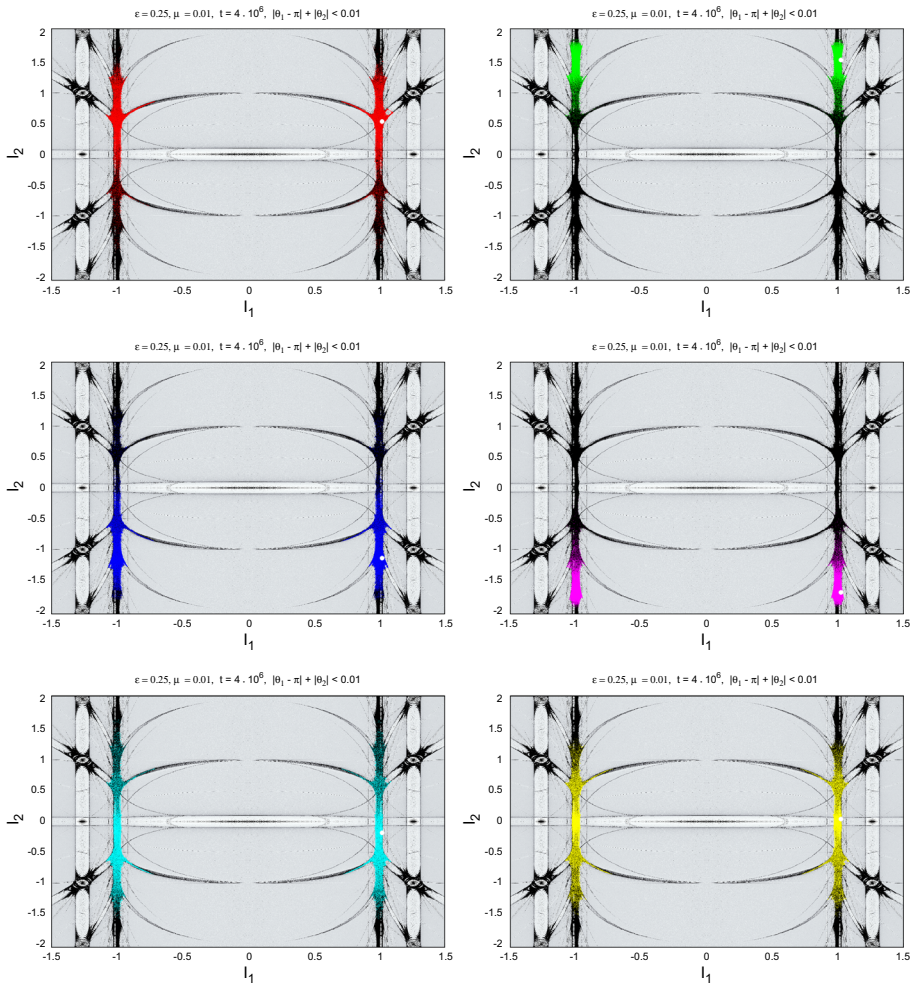
Fig. 8 Six initial ensembles (indicated as white circles) are followed onto the MEGNO contour plot and the concomitant trajectories depicted with different colors for $\mu = 0.01$
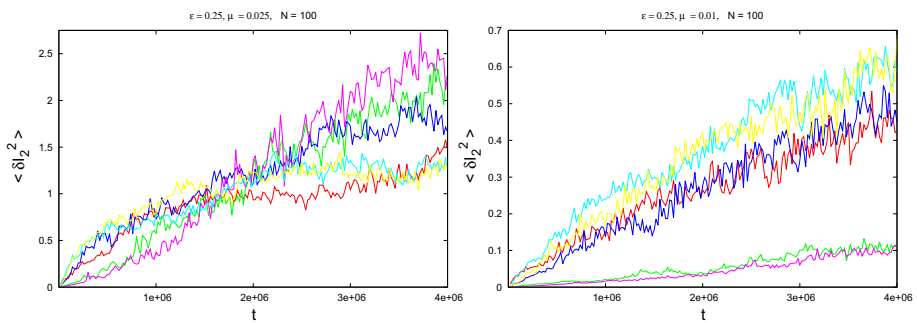

Fig. 9 Variance evolution $\langle \delta I_2^2 \rangle$ for the six ensembles with the same color identification for $\mu = 0.025$ (left) and $\mu = 0.01$ (right)
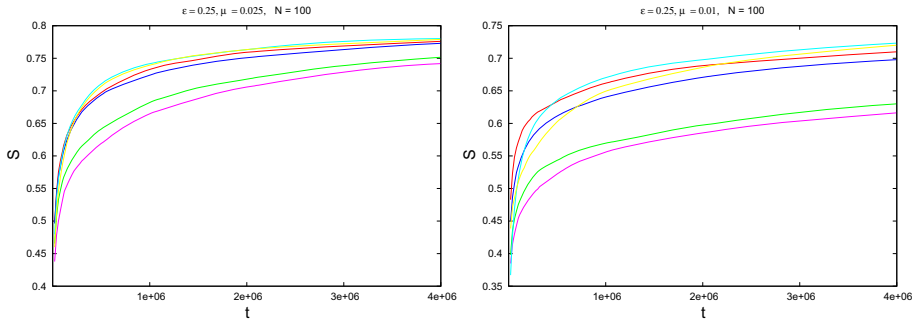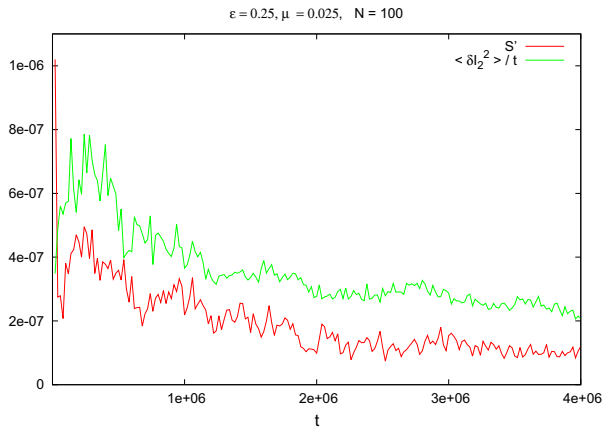
Fig. 10 Entropy, S, for the six ensembles with the same color identification for $\mu = 0.025$ (left) and $\mu = 0.01$ (right) for a partition $q = 400 \times 400$ over the domains $|I_1| \leq 1.4, |I_2| \leq 2.5$ for $\mu = 0.025$ and $|I_1| \leq 1.12, |I_2| \leq 2$ for $\mu = 0.01$

Fig. 11 Comparison of $\langle \delta I_2^2 \rangle / t$ and S' for the ensemble located at $\omega_2 = -1.13$ for $\mu = 0.025$

$1.12\}$, $L_2 = \{I_2 : |I_2| \leq 2\}$ for $\mu = 0.01$ being l_1 and l_2 the diameter of L_1 and L_2, respectively. Figure 10 shows the evolution of the entropy for all the ensembles when adopting a partition $q = 400 \times 400$. Both figures reveal a very similar trend for the entropies for $\mu = 0.025$, while for $\mu = 0.01$ the ensembles for which the diffusion is restricted to $0.4 \lesssim |I_2| < 2$, S reaches smaller values, as expected. For instance, for $\mu = 0.025$, after $t = 4 \times 10^6$, $S \approx 0.8$ and thus for the given partition it leads to a linear extension of the instability in I_2 of $\sim q^{(S-1)/2} l_2 \approx 1.5$, which is smaller but comparable to the observed one for all the ensembles.

Figure 11 corresponds to the ensemble located at $\omega_2 = -1.13$ (for $\mu = 0.025$) and displays a comparison between the evolution of S' (normalizing k to the extent of the area covered by the diffusion of this ensemble) with $\langle \delta I_2^2 \rangle / t$. Notice that while the latter is still decreasing at $t = 4 \times 10^6$, S' already reaches a nearly asymptotic value at $t = 2 \times 10^6$, though both quantities exhibit a comparable evolution and similar final values.

Finally, Fig. 12 shows the evolution of S' for all the ensembles and both values of μ. It turns out that for $\mu = 0.025$ all the ensembles present a very similar diffusion rate measured by S', of the order of 10^{-7}. On the other hand, for $\mu = 0.01$ the diffusion rates for the ensembles for which the diffusion spreads over nearly the same region are similar, $\sim 5 \times 10^{-8}$, while
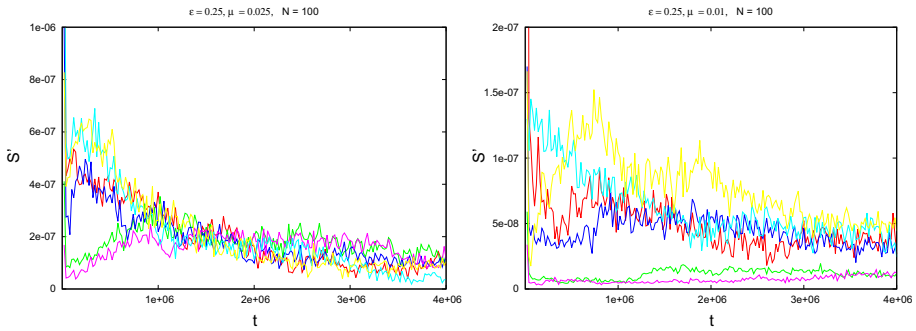
Fig. 12 S' for the six ensembles with the same color identification for $\mu = 0.025$ (left) and $\mu = 0.01$ (right) for a partition $q = 400 \times 400$ over the domains $|I_1| \leq 1.4$, $|I_2| \leq 2.5$ for $\mu = 0.025$ and $|I_1| \leq 1.12$, $|I_2| \leq 2$ for $\mu = 0.01$

those leading to a more restricted diffusion, also have comparable values, of the order of $\sim 10^{-8}$.

5 Conclusions

Herein we face the difficulty to compute a meaningful measure of the chaotic diffusion and its time rate, independent of the scaling of the variance with time. Theoretical, heuristic and numerical arguments support that S and S' are suitable estimators of diffusion in both limits, local and global diffusion. The strongest assumption for our proposal is indeed that the variation of the number of occupied cells is entirely due to changes in the actions during the diffusion process, while a second but weaker one regards the approximation of the actual entropy by the logarithm of the number of non-empty cells. A third though more natural assumption is the nearly equal measure of the cells occupied by the intersections of the ensemble trajectory with a given section. Anyway a more rigorous foundation of this formulation should be provided. We remark that the conjecture $\langle \delta y^2(t) \rangle \propto \delta q_0(t)$ is independent of the transport process that takes place in phase space and thus the time evolution of S and S' would reveal the character of the chaotic diffusion, i.e., normal or abnormal.

With the help of a 4D symplectic map and by recourse to the conditional entropy as indicator of chaos, we yield numerical evidence that S' gives reliable values of the mean diffusion rate within the domain covered by the roam of the action values, while S measures the extension of this domain, i.e., the range of variation of the actions over the considered time span.

For the sake of illustration, we have presented a few numerical examples involving chaotic diffusion of a single ensemble and the corresponding evolution of S, S_0, S' and the variances. However, plenty of computations have been carried out considering quite restricted diffusion, overlapping of several ensembles, dependence of the entropy on the adopted partition, different parameters of the map, etc. The outcomes presented in Sect. 3 tailor a quite representative sample of all our numerical experiments. Further, the global results displayed in Fig. 6 are pretty eloquent: both S and S' are very effective dynamical indicators (as follows from a simple comparison with Fig. 1); however, they also provide further information about the local and global dynamics than, for instance, the classical chaos indicators.

The application of this approach to chaotic diffusion in a well-known Hamiltonian system of more than two degrees of freedom reveals that our initial conclusions, that are based on profuse numerical experimentation on a 4D map, seem to be general and thus we claim for S and S' to characterize chaotic diffusion in phase space.

The computational effort to obtain the entropy and its derivative is nearly the same needed to evaluate the variances over the section, but of course it is quite large in comparison with the one required by any dynamical indicator of chaos. Indeed, in general, a dynamical indicator is computed for a given grid of individual initial conditions for relatively short motion times, while the entropy, as well as the variances, require a grid of initial ensembles and larger times. Anyway, when dealing with maps, this is not a serious limitation; however, it could be restrictive in the case of systems of continuous time and several degrees of freedom.

It turns out then that a combination of different techniques would furnish a very efficient way to investigate global and local dynamics in multidimensional systems. The structure of the phase space would be revealed by any chaos indicator, which would provide information on the location of invariant manifolds, resonances, stable and chaotic regions, etc., allowing to obtain a clear picture of the global dynamics of the model. However, since any classical indicator could not distinguish between stable or unstable chaos, S and S' should be computed in those chaotic domains of physical interest in order to get a measure of the instability and its time rate.

References

Arnold, V.I.: On the nonstability of dynamical systems with many degrees of freedom. Sov. Math. Dokl. **5**, 581–585 (1964)

Arnol'd, V., Avez, A.: Ergodic Problems of Classical Mechanics, 2nd edn. Addison-Wesley, New York (1989)

Batygin, K., Deck, K.M., Holman, M.J.: Dynamical evolution of multi-resonant systems: the case of GJ876. Astron. J. **149**, 167 (2015)

Cachucho, F., Cincotta, P.M., Ferraz-Mello, S.: Chirikov diffusion in the asteroidal three-body resonance (5, −2, −2). Celest. Mech. Dyn. Astron. **108**, 35 (2010)

Chandrasekhar, S.: Stochastic problems in physics and astronomy. Rev. Mod. Phys. **15**, 1 (1943)

Chirikov, B.V.: A universal instability of many-dimensional oscillator systems. Phys. Rep. **52**, 263 (1979)

Cincotta, P.M.: Astronomical time-series analysis-III. The role of the observational errors in the minimum entropy method. Mon. Not. R. Astron. Soc. **307**, 941 (1999)

Cincotta, P.M.: Arnold diffusion: an overview through dynamical astronomy. New Astron. Rev. **46**, 13–39 (2002)

Cincotta, P.M., Giordano, C.M.: Chaotic diffusion in multidimensional conservative maps. Int. J. Bifurc. Chaos **22**, 10 (2012)

Cincotta, P.M., Giordano, C.M.: Theory and applications of the Mean Exponential Growth Factor of Nearby Orbits (MEGNO) method. Lect. Notes Phys. **915**, 93 (2016)

Cincotta, P.M., Simó, C.: Conditional entropy. Celest. Mech. Dyn. Astron. **73**, 195 (1999)

Cincotta, P.M., Simó, C.: Simple tools to study global dynamics in non-axisymmetric galactic potentials-I. Astron. Astrophys. Suppl. Ser. **147**, 205 (2000)

Cincotta, P.M., Helmi, A., Méndez, M., Núñez, J.A., Vucetich, H.: Astronomical time-series analysis-II. A search for periodicity using the Shannon entropy. Mon. Not. R. Astron. Soc. **302**, 582 (1999)

Cincotta, P.M., Giordano, C.M., Simó, C.: Phase space structure of multi-dimensional systems by means of the mean exponential growth factor of nearby orbits. Physica D **182**, 11 (2003)

Cincotta, P.M., Efthymiopoulos, C., Giordano, C.M., Mestre, M.F.: Chirikov and Nekhoroshev diffusion estimates: bridging the two sides of the river. Physica D **266**, 49 (2014)

Cincotta, P.M., Giordano, C.M., Martí, J.G., Beaugé, C.: On the chaotic diffusion in multidimensional Hamiltonian systems. Celest. Mech. Dyn. Astron. **130**(1), 7 (2018)

Cordeiro, R.R.: Anomalous diffusion in the asteroid belt. Astron. J. **132**, 2114 (2006)

Cordeiro, R., Mendes de Souza, L.: Anomalous diffusion in the first-order Jovian resonance. Astron. Astrophys. **439**, 375 (2005)

Efthymiopoulos, C.: Canonical perturbation theory, stability and diffusion in Hamiltonian systems: applications in dynamical astronomy. In: Cincotta, P.M., Giordano, C.M., Efthymiopoulos, C. (eds.) Third La Plata International School on Astronomy and Geophysics: Chaos, Diffusion and Non-integrability in Hamiltonian Systems Applications to Astronomy (2012)

Efthymiopoulos, C., Harsoula, M.: The speed of Arnold diffusion. Physica D **251**, 19 (2013)

Fick, A.: Ueber diffusion. Ann. Phys. **95**, 59 (1855). **in German**

Froeschlé, C., Guzzo, M., Lega, E.: Local and global diffusion along resonant lines in discrete quasi-integrable dynamical systems. Celest. Mech. Dyn. Astron. **92**, 243 (2005)

Froeschlé, C., Lega, E., Guzzo, M.: Analysis of the chaotic behavior of orbits diffusing along the Arnold web. Celest. Mech. Dyn. Astron. **95**, 141 (2006)

Giorgilli, A.: New insights on the stability problem from recent results in classical perturbation theory. In: Benest, D., Froeschlé, C., (eds.) Les Methodes Modernes de la Mecanique Celeste. Frontières, pp. 249–284. ISBN: 2-8633209-2 (1990)

Katz, A.: Principles of Statistical Mechanics, The Information Theory Approach. W.H. Freeman & Co., San Francisco (1967)

Klafter, J., Blumen, A., Zumofen, G., Shlesinger, M.: Lévy walk approach to anomalous diffusion. Physica A **168**, 637 (1990)

Klafter, J., Zumofen, G., Shlesinger, M.: Lévy walks in dynamical systems. Physica A **200**, 222 (1993)

Korabel, N., Klages, R.: Microscopic chaos and transport in many-particle systems. Physica D **187**, 66 (2004)

Lega, E., Guzzo, M., Froeschlé, C.: Detection of Arnold diffusion in Hamiltonian systems. Physica D **182**, 179 (2003)

Lega, E., Froeschlé, C., Guzzo, M.: Diffusion in Hamiltonian quasi-integrable systems. Lect. Notes Phys. **729**, 29 (2008)

Lesne, A.: Shannon entropy: a rigorous notion at the crossroads between probability, information theory, dynamical systems and statistical physics. Math. Struct. Comput. Sci. **24**, e240311 (2014). https://doi.org/10.1017/S0960129512000783

Maffione, N.P., Gómez, F.A., Cincotta, P.M., Giordano, C.M., Cooper, A.P., O' Shea, B.W.: On the relevance of chaos for halo stars in the solar neighbourhood. Mon. Not. R. Astron. Soc. **453**, 2830 (2015)

Maffione, N.P., Gómez F.A., Cincotta, P.M., Giordano, C.M., Grand, R., Marinacci, F., et al.: On the relevance of chaos for halo stars in the solar neighbourhood II. Mon. Not. R. Astron. Soc. arXiv:1801.03946 (2018)

Martí, J.G., Cincotta, P.M., Beaugé, C.: Chaotic diffusion in the Gliese-876 planetary system. Mon. Not. R. Astron. Soc. **460**, 1094 (2016)

Miguel, N., Simó, C., Vieiro, A.: On the effect of islands in the diffusive properties of the standard map, for large parameter values. Found. Comput. Math. **15**, 89 (2014)

Tsiganis, K.: Chaotic diffusion of asteroids. Lect. Notes Phys. **729**, 111 (2008)

Tsiganis, K., Varvoglis, H., Dvorak, R.: Chaotic diffusion and effective stability of Jupiter Trojans. Celest. Mech. Dyn. Astron. **92**, 71 (2005)

Simó, C.: Global dynamics and fast indicators. In: Broer, H.W., Krauskopf, B., Vegter, G. (eds.) Global Analysis of Dynamical Systems, pp. 373–390. IOP Publishing, Bristol (2001)

Shannon, C., Weaver, W.: The Mathematical Theory of Communication. Illinois U.P., Urbana (1949)

Schwarzl, M., Godec, A., Metzler, R.: Quantifying non-ergodicity of anomalous diffusion with higher order moments. Sci. Rep. (2017). https://doi.org/10.1038/s41598-017-03712-x

Venegeroles, R.: Calculation of superdiffusion for the Chirikov–Taylor model. Phys. Rev. Lett. **101**, 54102 (2008)

Wehrl, A.: General properties of entropy. Rev. Mod. Phys. **50**(2), 221 (1978)

Zaslavsky, G.M.: Fractional kinetic equation for Hamiltonian chaos. Physica D **76**, 110 (1994)

Zaslavsky, G.M.: Chaos, fractional kinetics, and anomalous transport. Phys. Rep. **371**, 461 (2002a)

Zaslavsky, G.M.: Dynamical traps. Physica D **168–169**, 292 (2002b)

Zaslavsky, G.M., Abdullaev, S.S.: Scaling properties and anomalous transport of particles inside the stochastic layer. Phys. Rev. E **51**, 3901 (1995)

Zaslavsky, G.M., Edelman, M.: Hierarchical structures in the phase space and fractional kinetics: I. Classical systems. Chaos **10**, 135 (2000)

Zaslavsky, G.M., Niyazow, B.A.: Fractional kinetics and accelerator modes. Phys. Rep. **283**, 73 (1997)

Zaslavsky, G.M., Edelman, M., Niyazow, B.A.: Self-similarity, renormalization, and phase space nonuniformity of Hamiltonian chaotic dynamics. Chaos **7**, 159 (1997)

Zhou, J., Sun, Y., Zhou, L.: Evidence for Lévy random walks in the evolution of comets from the Oort cloud. Celest. Mech. Dyn. Astron. **84**, 409 (2002)